Magnetic Resonance in Medicine 46:713–722 (2001)

Sensitivity-Encoded Spectroscopic Imaging

Ulrike Dydak, Markus Weiger, Klaas P. Pruessmann, Dieter Meier, and Peter Boesiger*

Sensitivity encoding (SENSE) offers a new, highly effective approach to reducing the acquisition time in spectroscopic imaging (SI). In contrast to conventional fast SI techniques, which accelerate *k*-space sampling, this method permits reducing the number of phase encoding steps in each phase encoding dimension of conventional SI. Using a coil array for data acquisition, the missing encoding information is recovered exploiting knowledge of the distinct spatial sensitivities of the individual coil elements. In this work, SENSE is applied to 2D spectroscopic imaging. Fourfold reduction of scan time is achieved at preserved spectral and spatial resolution, maintaining a reasonable SNR. The basic properties of the proposed method are demonstrated by phantom experiments. The in vivo feasibility of SENSE-SI is verified by metabolic imaging of N-acetylaspartate, creatine, and choline in the human brain. These results are compared to conventional SI, with special attention to the spatial response and the SNR. Magn Reson Med 46:713–722, 2001. © 2001 Wiley-Liss, Inc.

Key words: fast spectroscopic imaging; SENSE; CSI; sensitivity encoding

In recent years, studies on the metabolism of the healthy and pathologic human brain are increasingly performed using proton magnetic resonance spectroscopic imaging (SI) (1–6). For the investigation of local metabolite concentrations, the advantage of SI over single voxel spectroscopy lies in the spatial resolution obtained by acquiring a whole grid of spectra. These spectra show only a slight reduction in the signal-to-noise ratio (SNR) per unit volume and unit time with respect to single voxel spectroscopy (7). Furthermore, displaying the resulting metabolite levels as images permits an easy comparison of local metabolism changes with other data, e.g., anatomical images and functional activation maps. The major disadvantage of standard SI techniques (8,9) is the long acquisition time of high-resolution measurements, which considerably complicates clinical application.

The long acquisition time of SI measurements with two spatial dimensions arises from the large number of samples to be collected, i.e., $K_x \times K_y \times N_t$ samples in the two spatial dimensions and one time/spectral dimension. In conventional spectroscopic imaging *k*-space is sampled by acquiring N_t data points in the time dimension per excitation, thus requiring $K_x \times K_y$ excitations for a complete 2D spatial image. In the past decade, several fast SI methods have been proposed in response to this problem, which rely on sampling *k*-space in a more time efficient way.

One fast SI technique, proposed by Duyn and Moonen (10), exploits the fact that at lower field strengths T_2 is much longer than T_2^* for the metabolites of interest, allowing one to acquire several spin-echoes per excitation, which are separately phase-encoded. The time savings achievable with this technique depend on the length of the spin-echo train, which typically ranges from 2 to 4. However, measurements with short echo spacing are not feasible with this technique, as the acquisition interval and thus the spectral resolution are limited by the echo spacing. Furthermore, acquiring multiple spin-echoes results in uneven T_2-weighting of *k*-space, which adversely affects the point-spread function of the technique. Another type of fast SI technique uses readout gradients for spatial encoding. Based on an SI method originally proposed by Mansfield (11), proton echo-planar spectroscopic imaging (PEPSI) by Posse et al. (12) saves time by acquiring $K_x \times N_t$ data points per excitation using echo-planar trajectories. A third option is the acquisition of $K_x \times K_y$ data points per excitation, as done in the typical Seppponen experiment (13), where the chemical shift information is encoded by incrementing the evolution period for each excitation. Several concepts known from fast MR imaging, such as echo-planar imaging (EPI), U-FLARE, and spiral acquisition, have been successfully applied for this purpose (14–16). In this case, the spatial resolution and the scan time can be varied independently, with the scan time determining the spectral resolution.

Throughout, these fast SI methods require sampling a full set of $K_x \times K_y \times N_t$ data points and achieve scan time reduction by accomplishing a greater number of samples per excitation. In this work, a new fast SI method is presented which takes a fundamentally different approach. It is based on the concept of sensitivity encoding (SENSE), originally described for fast MR imaging (17), which permits undersampling *k*-space by using multiple receiver coils for signal acquisition. In SENSE reconstruction, the spatial encoding information lost through undersampling is recovered using knowledge of the distinct individual coil sensitivities. By applying this concept to each spatial phase encoding dimension, the scan times required for spectroscopic imaging can be substantially reduced without compromising spatial or spectral resolution.

The basic concepts of sensitivity-encoded SI are explained in the Methods section. In order to evaluate the relative performance of the new technique, a comparison between 2D SENSE-SI and conventional 2D SI is presented, using both in vitro and in vivo experiments. In the phantom study, special attention is given to the specific SNR and spatial response behavior of SENSE-SI. The in vivo feasibility of the new technique is demonstrated by a brain study, yielding high-resolution maps of N-acetylaspartate, creatine, and choline concentration in one-fourth the conventional scan time.

METHODS

SENSE-SI

SENSE (17) utilizes spatial information related to the coil sensitivities of a receiver array for signal localization,

Institute for Biomedical Engineering, University of Zurich and Swiss Federal Institute of Technology Zurich, Zurich, Switzerland.

Grant sponsor: Swiss National Science Foundation; Grant number: 31-52173.97.

*Correspondence to: Prof. Dr. P. Boesiger, Institute for Biomedical Engineering, University and ETH Zurich, Gloriastrasse 35, CH-8092 Zurich, Switzerland.

Received 10 October 2000; revised 19 April 2001; accepted 19 April 2001.

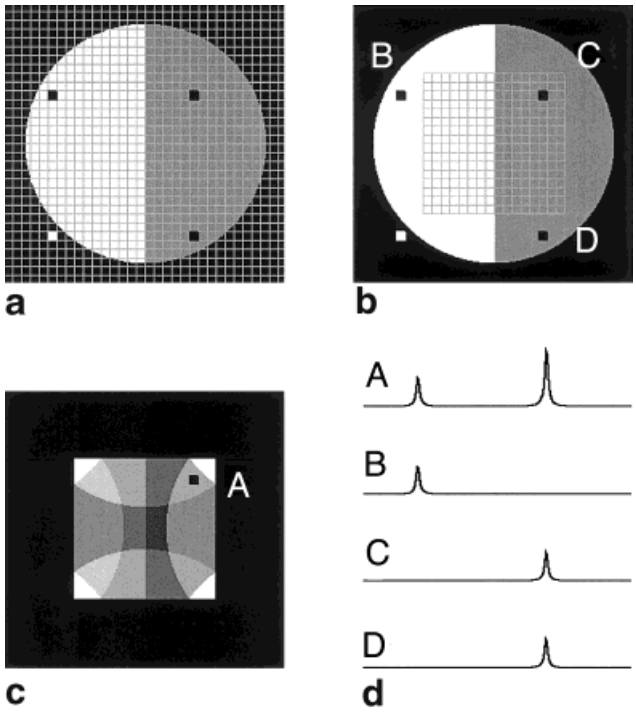

FIG. 1. Schematic representation of an object containing two different metabolites (white and gray compartment): For a SENSE experiment the full FOV of a conventional SI measurement with a grid of 32 × 32 pixels (**a**) is reduced by a factor two in both dimensions, covering only a 16 × 16 grid (**b**) with the same nominal spatial resolution. This way only every fourth point in *k*-space is sampled compared to full *k*-space sampling, leading to a scan time reduction of four. Applying Fourier reconstruction, such undersampling results in aliasing artifacts, as shown in **c**. Voxel A is the weighted sum of the four voxels depicted in **a** and **b**. Therefore, the spectrum of voxel A in **d** exhibits peaks at two frequencies corresponding to the weighted sum of the signals of the contributing voxels B, C, and D.

while using the homogeneous RF field of the body coil for excitation. This permits reducing the scan time by decreasing the sampling density in *k*-space, which is equivalent to reducing the field-of-view (FOV). The sensitivities of the receiver coils provide complementary information enabling image reconstruction free of aliasing artifacts, which would otherwise result from undersampling *k*-space. The minimal number of receiver channels required for such a reconstruction is given by the reduction factor of *k*-space sampling density.

For most efficient scan time reduction in conventional SI, the SENSE method can be applied to both spatial phase encoding dimensions, x and y (18). For a SENSE-SI experiment the FOV is reduced by a factor R_x in *x* direction and a factor R_y in *y* direction. In this fashion, only a fraction of *k*-space positions is sampled as compared with full *k*-space sampling, leading to scan time reduction by the factor $R = R_x \times R_y$. Thus, if the full FOV is to be resolved by $n \times n$ spectra (Fig. 1a), only $n/R_x \times n/R_y$ individual signals need to be sampled. In the imaging domain, this sampling scheme corresponds to an $n/R_x \times n/R_y$ grid within a reduced FOV (Fig. 1b).

Figure 1c shows the aliasing artifacts after conventional Fourier reconstruction resulting from such undersampling. Each voxel in the reduced FOV represents the weighted signal sum of four voxels in the full FOV. Thus, one spectrum from the reduced FOV will contain metabolite peaks originating from any of these four locations (Fig. 1d). In order to create full-FOV metabolite maps, these signal contributions need to be separated. This is achieved by SENSE reconstruction, which exploits the fact that each signal contribution is weighted according to the local sensitivity of the respective coil. With two spatial and one frequency dimension, the basic SENSE-SI experiment is similar to 2D SENSE (19), as the spectral encoding of the frequency dimension by the chemical shift can be viewed as equivalent to spatial encoding with magnetic field gradients. Thus, the spectral dimension is simply treated as a third dimension with no undersampling. After discrete Fourier transform in all three dimensions, an aliased image needs to be unfolded for every sampling frequency in the spectral direction. Consider one voxel in the reduced FOV, and the corresponding set of voxels in the full FOV (Fig. 1b). Following the notation used in Ref. 17, let *S* denote the *sensitivity matrix*, containing the spatial sensitivity of each coil for each superimposed voxel position. Then the *unfolding matrix U* is given by:

$$U = (S^H \Psi^{-1} S)^{-1} S^H \Psi^{-1}, \quad [1]$$

where the superscript *H* denotes the transposed complex conjugate and Ψ is the receiver noise matrix, describing the levels and correlation of noise in the receiver channels. The matrix Ψ is determined experimentally, using:

$$\Psi_{\gamma,\gamma'} = \overline{\eta_\gamma \eta^*_{\gamma'}}, \quad [2]$$

where η_γ denotes the pure noise output of the γ-th receiver channel, the bar denotes time averaging, and the asterisk denotes the complex conjugate. Note that Eq. [2] is statistically equivalent to eq. A9 in Ref. 17.

For each spectral sampling point λ, signal separation is achieved by:

$$\mathbf{v}_\lambda = U\mathbf{a}_\lambda, \quad [3]$$

where the vector $\mathbf{a}_\lambda$ lists the complex image values of the chosen voxel in the aliased images obtained by each coil, and the resulting vector $\mathbf{v}_\lambda$ lists the separated voxel values for the originally superimposed voxels in the full-FOV. This procedure is repeated for each voxel in the reduced FOV to obtain a full image, and for each λ in spectral direction to obtain a full spectroscopic imaging dataset. As a result, each spectrum only shows peaks of metabolites actually contained in the corresponding full-FOV voxel (Fig. 1d).

Spatial Response Function

Closely related to the point spread function (PSF), the spatial response function (SRF) of a voxel is a spatial weighting function describing the signal origin in that voxel and is identical to the *voxel function* described in Ref. 17. As signals of different spatial origin are separated in SENSE reconstruction, the behavior of the SRF becomes

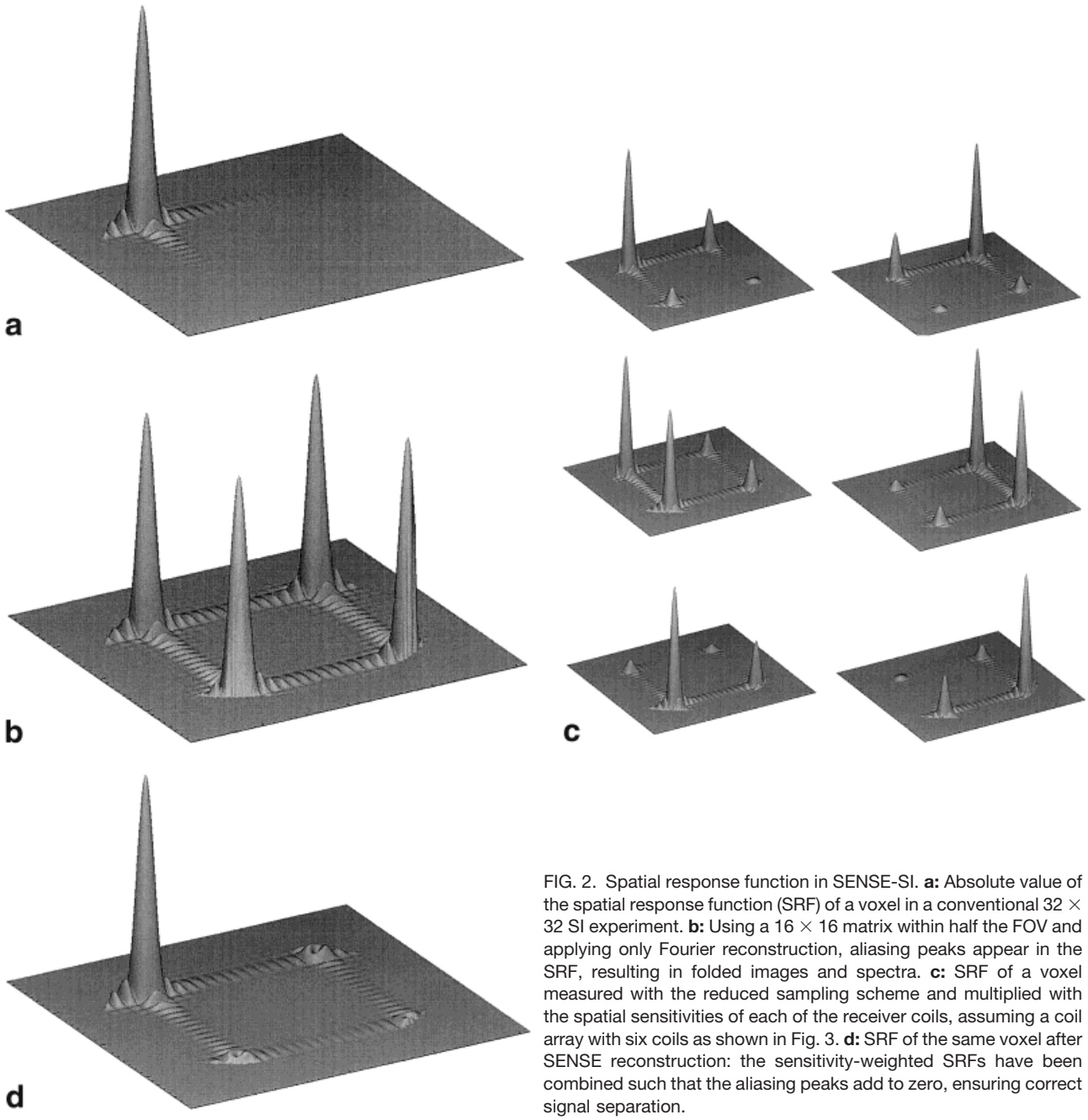

FIG. 2. Spatial response function in SENSE-SI. **a:** Absolute value of the spatial response function (SRF) of a voxel in a conventional 32 × 32 SI experiment. **b:** Using a 16 × 16 matrix within half the FOV and applying only Fourier reconstruction, aliasing peaks appear in the SRF, resulting in folded images and spectra. **c:** SRF of a voxel measured with the reduced sampling scheme and multiplied with the spatial sensitivities of each of the receiver coils, assuming a coil array with six coils as shown in Fig. 3. **d:** SRF of the same voxel after SENSE reconstruction: the sensitivity-weighted SRFs have been combined such that the aliasing peaks add to zero, ensuring correct signal separation.

particularly important. Using spatial sensitivities of coil array elements for image reconstruction, in SENSE-SI the spatial response function also depends to some degree on sensitivity relations and varies slightly from voxel to voxel.

For a conventional SI image the SRF is essentially a sinc-shape, as associated with the Fourier transformation of the limited *k*-space sampling area (Fig. 2a). However, the side lobes of the sinc-function are reduced by a cosine filter, applied to the spatial *k*-space dimensions. Due to the discrete fashion of the sampling, this modified sinc-function is repeated in space with a periodicity corresponding to the FOV. After undersampling, the SRF of each voxel in the reduced FOV exhibits multiple peaks within the original FOV (Fig. 2b), corresponding to aliasing. Multiplying the SRF of an exemplary voxel with each of the coil sensitivities yields the SRFs of the respective voxel in the aliased images as obtained from each coil (Fig. 2c). The spatial response of the voxel x,y in the final dataset is then obtained by applying SENSE reconstruction to the sensitivity weighted SRFs:

$$\mathrm{SRF}_{x,y}(\mathbf{r}) = \sum_{\gamma} U_{\rho,\gamma} \cdot \mathrm{sinc}_{x,y}(\mathbf{r}) \cdot s_{\gamma}(\mathbf{r}). \qquad [4]$$

Here, ρ denotes the index of the voxel (x,y) under consideration within the set of voxels to be separated (for a

reduction factor $R = 4$, e.g., $\rho = 1, \ldots, 4$), λ counts the coils and $s_\lambda(\mathbf{r})$ is the complex spatial sensitivity of the coil λ. U is the unfolding matrix as defined in Eq. [1] and the sinc-function, centered in the voxel x,y, is periodic according to the reduced FOV.

By the unfolding matrix, the weighting coefficients for each voxel are chosen such that aliasing peaks within the imaged object add to zero (Fig. 2d). The actual degree of aliasing of a particular voxel is determined by the SENSE reduction factor R, the size of the object, and the location of the voxel. For two reasons SENSE reconstruction is performed only for voxels within the object border: first, the sensitivity outside the object cannot be readily assessed; second, reducing the degree of aliasing improves the SNR (17). However, as will be seen in the Results section, it is advisable to extend the sensitivities and the reconstruction somewhat beyond the object border. If a voxel has one of its aliasing peaks just outside the object border, the signal contribution from the tail or first side lobes of that aliasing peak may be larger than in conventional SI and may lead to visible artifacts. Therefore, voxels within one side lobe off the object border should also be reconstructed on the basis of slightly extrapolated sensitivities, such that aliasing peaks at these locations approximately add to zero as well.

Signal-to-Noise Ratio

The propagation of white noise in SENSE reconstruction was previously studied in Ref. 17. According to that analysis, the SNR in a SENSE dataset compares with that obtained by full Fourier encoding according to:

$$\mathrm{SNR}_{\mathrm{SENSE}} = \frac{\mathrm{SNR}_{\mathrm{conv}}}{g\sqrt{R}}, \quad g \geq 1 \qquad [5]$$

where $R = R_x \times R_y$ denotes the net reduction factor, and g denotes the local geometry factor, which depends on the shape, size, and placement of the receiver coils. The geometry factor describes the ability of the coil configuration to separate pixels superimposed by aliasing and is optimally equal to 1. In an SI experiment, the SNR of the metabolite images closely relates to the SNR of the spectra, thus only the SNR of spectra is discussed here.

In order to compare the SNR of conventional SI spectra with that of the corresponding SENSE-SI spectra, the following definitions were used: The signal of a peak is given by the integral of the absolute data values over the peak interval, as used for calculating the metabolite images. Peak intervals were chosen 0.2 ppm wide and symmetrical around the peak's maximum. As the spectra were not fitted for data analysis, the integral provides more reliable values than the peak amplitude. The noise level was defined as the standard deviation of the real part of the data samples in a noise interval, which was chosen between 9.42 and 7.13 ppm. SNR evaluations were performed after all postprocessing, so the noise determination was based on a corrected baseline. The SNR of a metabolite peak, $\mathrm{SNR}_{\mathrm{peak}}$, is then defined as the ratio of S/N with:

$$\mathrm{signal} = \sum |x_i| \quad \text{and}$$

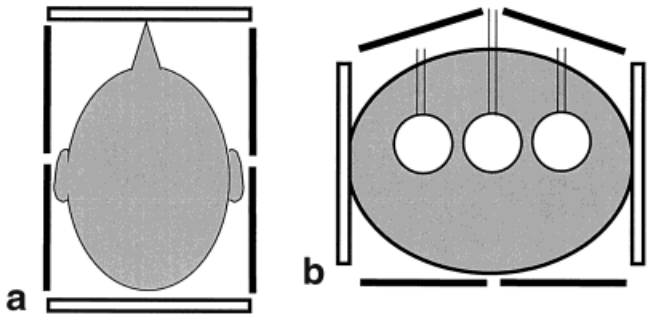

FIG. 3. Experimental setup of the coil array in vivo (**a**) and in the phantom experiment (**b**). Solid black lines represent rectangular elements (10 × 20 cm), void lines represent circular elements (diameter = 20 cm).

$$\mathrm{noise} = \sigma(\mathrm{noise}) \cdot \sqrt{N_{\mathrm{signal}}} = \sqrt{\frac{\sum_i \mathrm{Re}(x_i)^2}{N_{\mathrm{noise}}}} \cdot \sqrt{N_{\mathrm{signal}}} \qquad [6]$$

where N_{signal} is the number of samples in the peak interval, N_{noise} is the number of samples in the noise interval, and x_i denotes the complex spectrum data.

Experimental Setup

The receiver coil array consists of six elements, two of which are circular, with a diameter of 20 cm. The other four elements are rectangular with dimensions 10 × 20 cm. The placement of these coils with respect to each other and to the object was chosen such that the geometry factor described above was close to 1, corresponding to minimal loss in SNR. In vivo the two circular elements were placed in anterior and posterior position, with the rectangular elements arranged in pairs to the left and right of the head (Fig. 3a). For the phantom experiment, the arrangement was rotated by 90°, such that the circular elements covered the left and right sides and the rectangular elements the anterior and posterior sides of the phantom (Fig. 3b).

The phantom used is an elliptically shaped acrylic tank ($150 \times 200 \times 225$ mm^3), with three glass spheres (diameter = 40 mm) mounted inside, which can be filled with different metabolic solutions (20). The glass spheres contained a 10 mmol/l solution of N-acetylaspartate (NAA), a 20 mmol/l solution of creatine (CRE), and a 10 mmol/l lactate (LAC) solution respectively, while the tank was filled with a 10 mmol/l creatine solution. Electrical conductivity, relaxation times, and the pH value were adjusted to in vivo conditions by adding potassium chloride, nickel chloride, and caustic soda or hydrochloric acid. Because of the elliptic shape of the phantom, the homogeneity of the magnetic field is disturbed only slightly and in a similar fashion as by a human head.

Acquisition Protocol and Data Processing

Spectroscopic imaging data was obtained from healthy volunteers as well as from the phantom using a 1.5 T

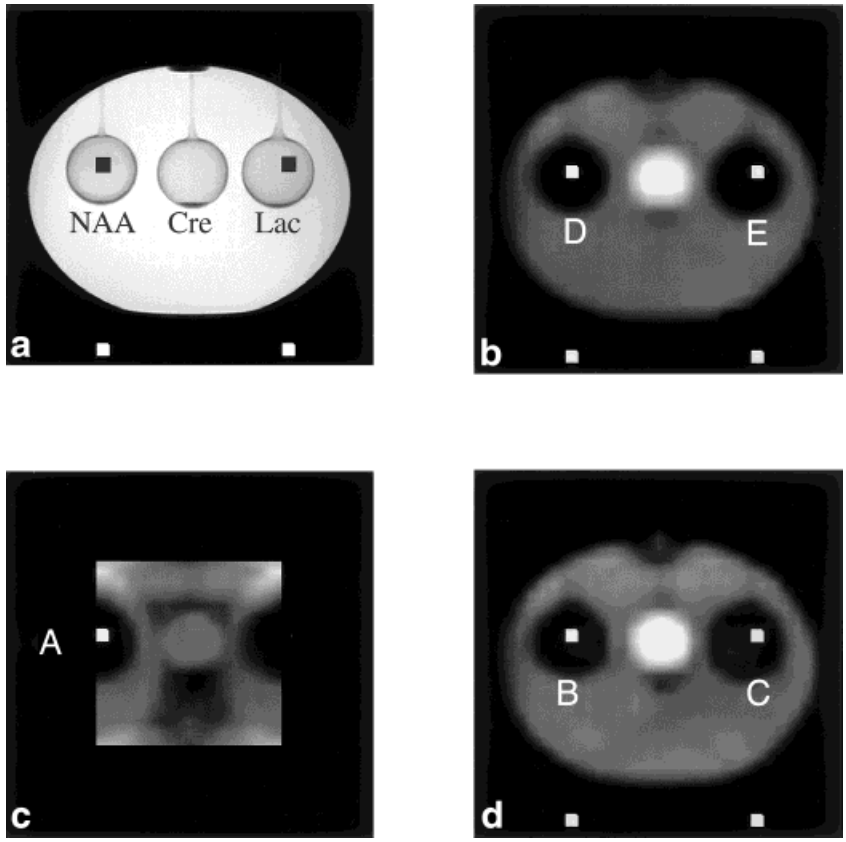

FIG. 4. In vitro results. **a:** The phantom was filled with a creatine solution of 10 mmol/l concentration and the glass spheres were filled from left to right with NAA (10 mmol/l), creatine (20 mmol/l), and lactate (10 mmol/l). **b:** The creatine map of the slice depicted in **a**, acquired with conventional SI in 26 min. The creatine map of the same slice acquired with half the FOV in only 6.5 min is shown without SENSE reconstruction in **c**, exhibiting aliasing artifacts due to undersampling. With SENSE reconstruction the foldover is removed (**d**). Voxels A–D are explained in Fig. 5.

Philips Gyroscan ACS-NT whole body scanner. In each experiment a conventional SI measurement was followed by a SENSE-SI measurement. The sensitivity information needed for SENSE reconstruction was obtained as in the original SENSE procedure from a reference scan, acquiring an image of the slice to be examined with each of the surface coils simultaneously, and the body coil. This reference scan has to be performed with exactly the same geometrical setup as chosen for the SI experiment.

For conventional SI, 32×32 spectra were obtained from a square FOV of 230 mm^2. For the SENSE experiment with a reduction factor of $R_x = R_y = 2$, only 16×16 spectra needed to be acquired. The FOV was reduced by a factor two in each phase encoding dimension, thus maintaining the nominal spatial resolution. A chemical shift selective saturation (CHESS) sequence (21) was used for water suppression. Subcutaneous fat was suppressed by an outer volume suppression technique, as described in Ref. 10, consisting of 10–12 presaturated slabs covering the skull. In vivo, a volume of interest (VOI) of $169 \times 120 \times 25$ mm^3 was selected by the PRESS sequence (22). In the phantom experiments the VOI was chosen equal to the FOV. Per repetition time (TR = 1500 ms) one echo (TE = 136 ms) with 512 samples was acquired using a bandwidth of 750 Hz, resulting in a spectral resolution of 1.5 Hz. Before each SI measurement a B_0-map was acquired with half the spatial resolution to enable correction for B_0-inhomogeneities in the postprocessing of the data. The B_0-map in the SENSE case was also measured with half the FOV and reconstructed with the SENSE algorithm.

SI data from the full and reduced FOV, respectively, was obtained simultaneously with each of the six surface coil channels. Besides the SENSE reconstruction, all postprocessing was identical for the conventional and the SENSE-SI data. First a cosine *k*-space filter was applied to the dataset of each coil. Next, the six datasets were combined to one full-FOV dataset either by sensitivity-corrected summation in the case of conventional spectroscopic imaging, or by using the SENSE reconstruction algorithm. Further data processing of the reconstructed full-FOV dataset comprised the B_0-correction and an exponential time filter. Reduction of the residual water signal was achieved by shifting all FIDs over several points and subtracting these from the originals. The signals with zero frequency, the water frequency, are nulled in this fashion. Thereafter, zero order phase correction and polynomial baseline correction in the frequency domain were applied to all spectra. Metabolite images were obtained by integrating the spectra over the modulus peak belonging to that specific metabolite in each voxel. A resolution of 256×256 pixels was attained by Fourier interpolation. In vivo NAA, creatine plus phosphocreatine (CRE), and choline-containing compounds (CHO) maps were investigated, while the phantom supplied NAA, creatine, and lactate images.

RESULTS

Phantom Experiments

Figure 4 shows results from the phantom experiment, demonstrating that spectra and image voxels superimposed by aliasing are separated with the SENSE algorithm. Figure 4b shows the creatine map of the slice

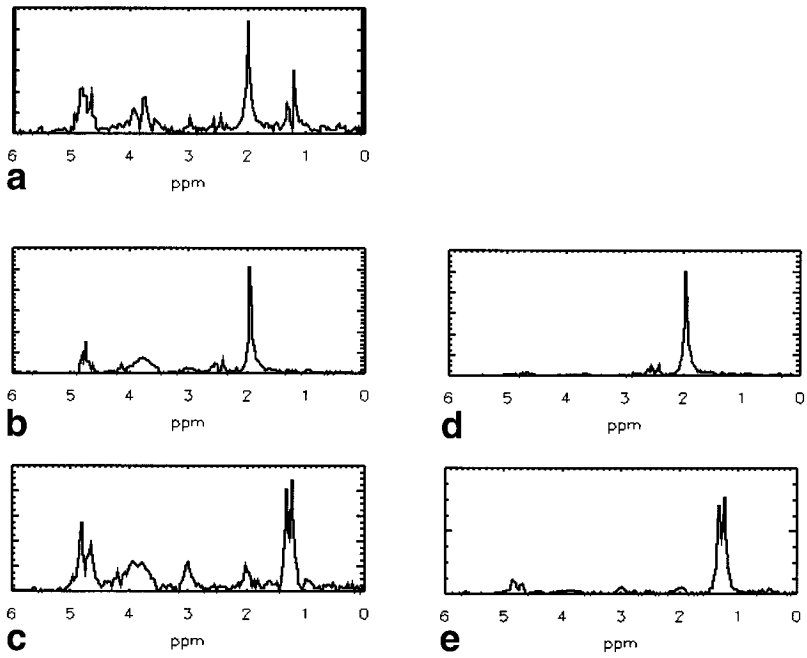

FIG. 5. **a:** Due to undersampling, spectrum A from voxel A in Fig. 4 is the weighted sum of the spectra from the four voxels shown in the full images. Signal from NAA as well as from lactate and poorly suppressed water can be distinguished. The two contributing spectra, shown after SENSE reconstruction, are spectrum B from voxel B (**b**), containing NAA, and spectrum C from voxel C (**c**) containing lactate. For comparison, spectra D (**d**) and E (**e**) show the same voxels as B and C, but have been acquired with full phase encoding.

depicted in Fig. 4a acquired with conventional SI in 26 min. The creatine map of the same slice acquired with half the FOV in only 6.5 min is shown without SENSE reconstruction in Fig. 4c, exhibiting aliasing artifacts due to undersampling. With SENSE reconstruction the foldover is removed (Fig. 4d).

Figure 5 shows the spectra of the voxels labeled in Fig. 4. Due to undersampling in the spatial dimensions, the spectrum of voxel A (Figs. 4c, 5a) represents a weighted sum of the spectra of the four voxels shown in the full images. Thus it contains signal both from the NAA-sphere as well as from the LAC-sphere (black voxels in Fig. 4a). The other two voxels (white) lie outside the phantom and do not contribute to the signal. After SENSE reconstruction the two contributing spectra, spectrum B (Fig. 5b), containing NAA, and spectrum C (Fig. 5c), containing LAC, are separated. For comparison, spectra D and E in Fig. 5d,e show spectra from the same locations as B and C, but were acquired with conventional SI. SENSE and conventionally acquired spectra are scaled differently according to their maximum amplitude: residual water peaks as well as, e.g., residual NAA and CRE peaks in Fig. 5c, appear more prominent in SENSE spectra than in conventional spectra. These residual metabolite peaks are not due to unfolding imperfections, but stem from the spatial response function, which displays larger side lobes in the SENSE case and thus leads to increased contamination. However, such contamination can also be observed in conventional SI, when the side lobes of the SRF do not cancel out due to sharp edges.

Signal-to-Noise Ratio

In the phantom experiment, two metabolite peaks, NAA at 2.02 ppm and LAC at 1.3 ppm, were evaluated for SNR. Voxel B and C from Fig. 4, both centered in a glass sphere filled with NAA or LAC, respectively, were compared between conventional SI and SENSE-SI. Table 1 summa-

Table 1
SNR of Metabolite Peaks in Corresponding Voxels in SENSE-SI Compared to Conventional SI

	$SNR_{conv.}$	SNR_{SENSE}	$\frac{SNR_{conv.}}{SNR_{SENSE}}$	Geometry factor g	$g * \sqrt{R}$
Phantom (Fig. 4)					
voxel B (NAA)	227	108	2.11 ± 0.14	1.008	2.02
voxel C (Lac)	114	55	2.07 ± 0.09	1.009	2.02
In vivo (Fig. 7)					
black voxel (NAA)	136	63	2.16	1.052	2.10
black voxel (Cre)	65	28	2.32	1.052	2.10
black voxel (Cho)	71	37	1.92	1.052	2.10

The table lists the SNRs of three voxels: SNR_{NAA} of voxel B (Fig. 4) and SNR_{Lac} of voxel C (Fig. 4) in the phantom measurements, and SNR_{NAA}, SNR_{CRE}, and SNR_{CHO} of the voxel shown in black in Fig. 7 (in vivo). It can be seen that the factor $g \cdot \sqrt{R}$, as obtained from Eq. [5], gives a good approximation for the ratio of $SNR_{conv.}$ to SNR_{SENSE}. In the phantom experiment four equivalent SENSE measurements were evaluated for SNR. Thus, it was possible to give an approximation for the error of the ratio. Although $SNR_{conv.}$ and SNR_{SENSE} are rounded numbers in this table, the ratio is calculated with the exact numbers.

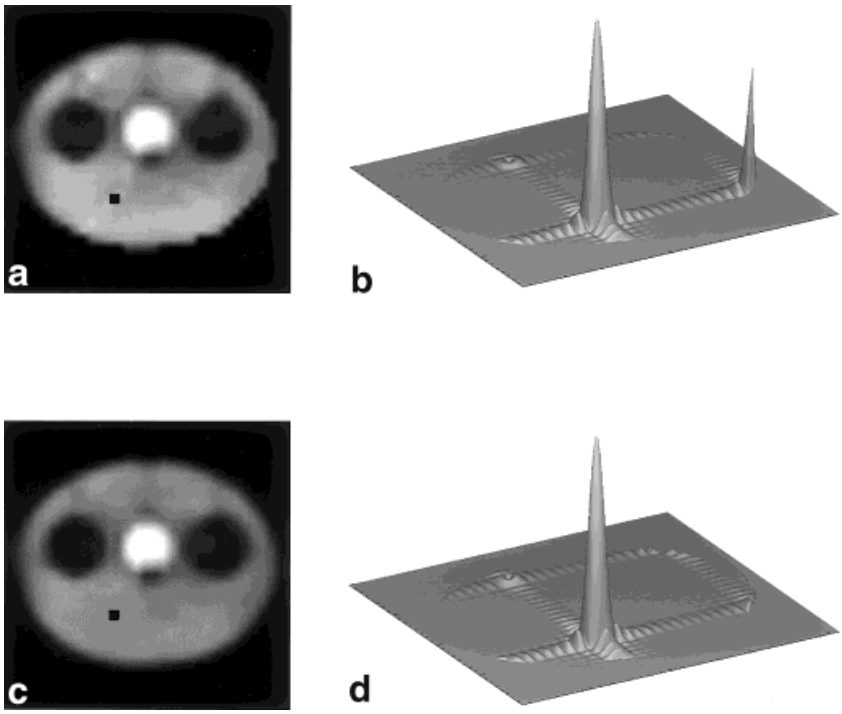

FIG. 6. **a:** Creatine map showing a foldover artifact in a SENSE-SI experiment, caused by the tail of an aliasing peak which is just outside the object and thus ignored by the reconstruction algorithm. **b:** Spatial response function (SRF) of the black voxel depicted in **a**. **c:** Creatine map of the same SENSE-SI measurement, yet with SENSE reconstruction including several voxels beyond the object borders. **d:** SRF of the black voxel in **c**, the critical alias peak is suppressed. Side lobes are attenuated in the neighborhood; however, partly enhanced in other regions.

rizes the peak-specific SNR for those voxels in the conventional and the SENSE-SI case, respectively. The signal interval for the SNR evaluation was chosen to be nine sample points or 0.2 ppm around the peak of interest. The noise interval contained 100 sample points (2.3 ppm). The SENSE experiment was repeated four times for an estimation of the error. All values given for the SENSE experiment are mean values of these four measurements and errors are given by the SD. Next to the values found experimentally, the theoretical value for the ratio $SNR_{conv.}/SNR_{SENSE}$ with white noise, $g \cdot \sqrt{R}$, according to Eq. [5], is listed in the last column for each voxel. R denotes the SENSE reduction factor, in our case four, and g stands for the geometry factor as described in the Methods section. For both voxels the experimental value is well predicted by theory. The SNR loss in SENSE-SI with optimized coil geometry is entirely accounted for by the reduction in sample points: With a SENSE reduction factor of four it is shown that the loss in SNR is a factor of two.

Spatial Response Function

Creatine maps reconstructed from the same SENSE-SI measurement with different extensions of the object border are displayed in Fig. 6. Figure 6b shows the absolute value of the complex spatial response function of the black voxel from Fig. 6a. It can be seen that for this specific voxel the SRF causes a problem, as an aliasing peak is located just outside the imaged object. Without extrapolation of the reconstruction beyond the object border, this aliasing is ignored by the reconstruction algorithm, which results in large side lobes and tails from the aliasing peak inside the object, as seen in Fig. 6b. Large signal at the location of these side lobes causes image artifacts (Fig. 6a). Figure 6d shows the SRF of the same SENSE-SI voxel as Fig. 6b, but with several voxels outside the object included in the reconstruction. In this fashion also the alias peaks just outside the object are forced to be zero and the contributions from their neighborhood are suppressed. Thus, the aliasing artifacts disappear, as demonstrated in Fig. 6c.

In Vivo Experiments

In vivo experiments were performed on a healthy volunteer. For one slice of the brain (Fig. 7a), first a conventional SI experiment was acquired, taking 26 min, which included 4 min for the B_0-map. The following SENSE-SI measurement lasted 6.5 min, including 1 min for the B_0-map. NAA, CRE (peak at 3.1ppm) and CHO images, interpolated to 256 × 256 pixels, are shown in Fig. 7 for both acquisition methods. The straight contours of the metabolite images are caused by the saturation slabs placed around the skull. Spectra from the black voxel are depicted in Fig. 8.

The SNR of the NAA, CRE, and CHO peaks was evaluated for the black voxel shown in Fig. 7 and listed in Table 1. As for the phantom case, the factor of loss in SNR is close to two and is well described by $\sqrt{R}$, with g close to 1.

DISCUSSION

Significant savings in scan time can be achieved by applying the SENSE technique to spectroscopic imaging. Having two phase encoding dimensions in conventional 2D SI and a SENSE reduction factor of two in both dimensions, the sampling density of k-space is reduced by a factor of four, reducing the scan time from 26 min to 6.5 min for a 32 × 32 SI experiment. This time reduction also helps in reducing problems related to patient motion. As can be seen in Fig. 7, metabolite images acquired with SENSE-SI are in good agreement with conventional metabolite images. NAA images are virtually identical. Ventricles are well

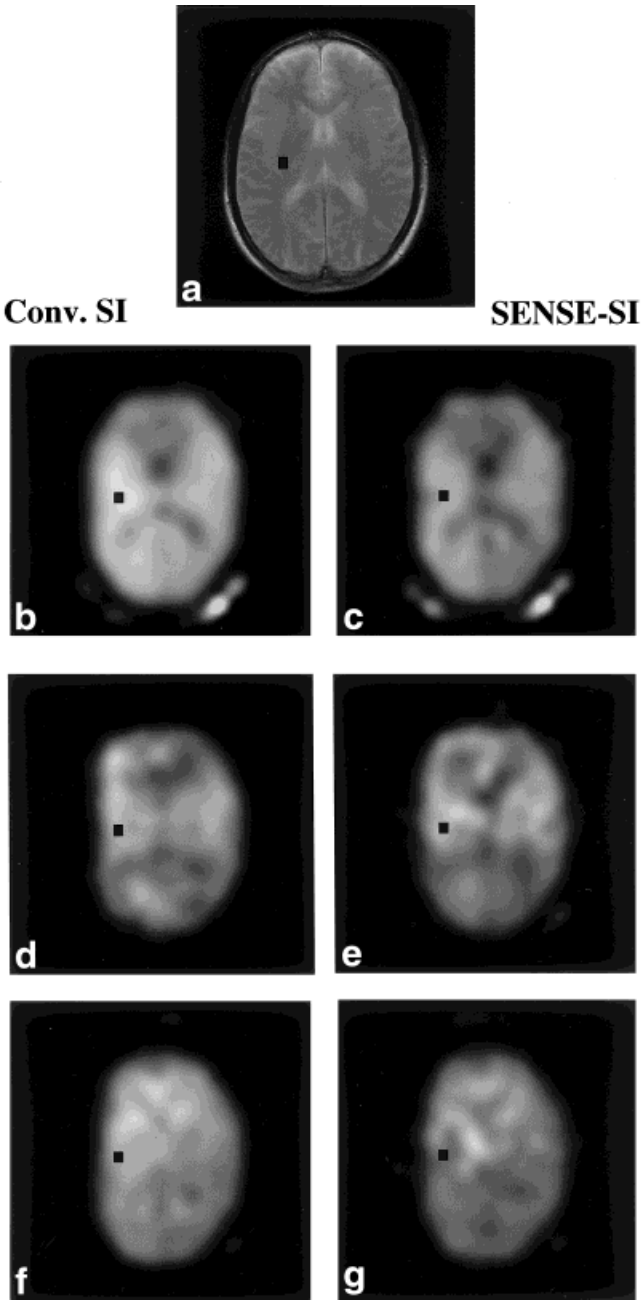

FIG. 7. In vivo results. Comparison of 32 × 32 metabolite images from the slice shown in **a:** The metabolite maps on the left hand side — (**b**) NAA, (**d**) CRE, and (**f**) CHO — were acquired with conventional SI in 26 min. The images on the right hand side — (**c**) NAA, (**e**) CRE, and (**g**) CHO — were acquired with SENSE-SI within 6.5 min. All metabolite images were interpolated to 256 × 256 pixels.

discernible and though the fat suppression was not completely successful, no aliasing of the lipid signals was found in the SENSE spectroscopic images. CRE and CHO images agree in key features, yet slight differences are observable due to the lower SNR and the different spatial response function. Artifacts due to the spatial response function in spectroscopic imaging in general, combined with the lower SNR in SENSE-SI, are especially visible in phantom studies with large concentration differences and sharp edges.

Reducing the acquisition time always brings about a reduction of the SNR. However, considering Gaussian noise, the SNR per unit volume and per unit time in SENSE-SI remains equal to that in conventional SI, except for the factor $1/g$. This geometry factor was optimized by the placement of the coils, such that g nearly equals 1.

Many other fast methods exhibit loss in spectral resolution and/or restrictions in the chosen spectral bandwidth or echo time. No parameter restrictions of any kind are necessary to achieve time-saving in SENSE-SI, and both spectral as well as spatial resolution are maintained. Neither does this method show increased sensitivity to lipid contamination. The SENSE reduction factor can be chosen independently for each dimension, compromising between scan time reduction and SNR. Furthermore, the extension to 3D SI with a sampling reduction of $R = R_x \times R_y \times R_z$ is straightforward, as the third phase encoding dimension can be undersampled accordingly, leading to R-fold scan time reduction. For this purpose, a minimum of R coils would be necessary and a suitable coil placement has to be found in order to keep the geometry factor close to 1. Alternatively, the reduced acquisition time of SENSE-SI may permit 2D kinetic studies in cases where changes of metabolite concentration over time are of interest.

An important additional advantage of SENSE-SI is its character of being a multicoil acquisition rather than a specific pulse sequence. This allows combining it with other fast SI methods. Applying SENSE to any fast SI method with spatial phase encoding will reduce the scan time by the SENSE reduction factor. One candidate is spectroscopic imaging with multiple echoes, where the scan time is first reduced by the number of echoes acquired and then by an additional factor four when combining it with SENSE (23). Other fast SI techniques would not become faster, but might gain spatial resolution.

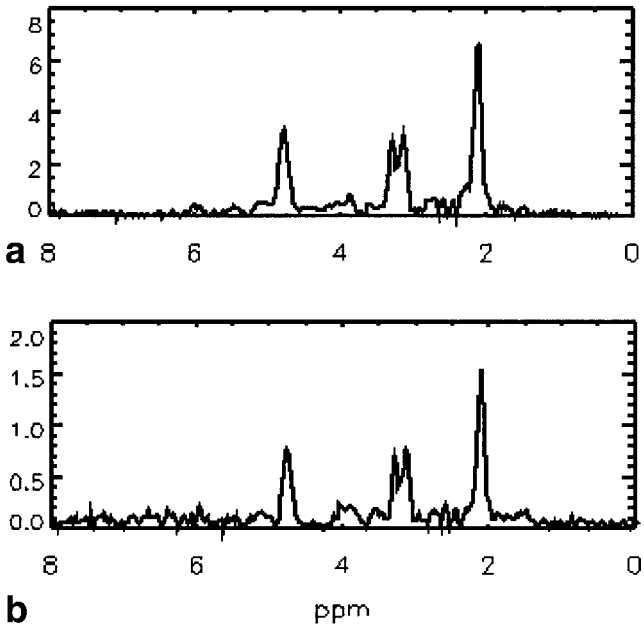

FIG. 8. ^{1}H Spectrum from the black voxel depicted in Fig. 7, acquired with conventional SI (**a**) and with SENSE-SI (**b**). The only discernible difference is the lower SNR in **b**.

In fast SI techniques, which encode the chemical shift with the method described by Sepponen (13), the scan time depends on the number of spectral samples acquired. Within each repetition time a full image is acquired with a fast imaging method for each chemical shift encoding. SENSE would allow acquiring images with higher spatial resolution when combined with any of these methods. However, when combining the speed benefits of multiple fast methods it has to be kept in mind that the SNR is generally governed by the square root of the total acquisition time. The trade-off between reduction in scan time and loss in SNR has to be considered for a reasonable choice of the SENSE reduction factor. This consideration must include the aim of a study, as well as the geometry of the object, the metabolite of interest, the available time for the measurement, or any other specific situation.

Furthermore, an optimized coil array can improve the overall SNR in SENSE-SI. As the size of our coil array elements is not yet optimized for measurements of the head, improvements of SNR are likely with a specific head coil array, as has been shown in other works (20). In the SENSE case a careful design of an optimized coil has to take into account not only noise coupling but also maintaining the *g*-factor optimal (24).

For a correct reconstruction of a metabolite image in SENSE-SI, the behavior of the spatial response function has to be considered. As shown in Fig. 6, the reconstruction parameters play a vital role in the behavior of the SRF of certain voxel. Extending the reconstruction several voxels beyond the object border improves the result considerably. In finding an optimal extension of the reconstruction, one has to consider that minor side lobes are slightly enhanced whenever major side lobes are suppressed. Therefore, the best reconstruction parameters also depend on the actual shape and size of the object to be imaged.

Applying sensitivity encoding to multislice SI techniques will be even more efficient regarding scan time. As the low concentrations of the metabolites investigated require a minimal repetition time of 1.5–2 sec in order not to lose signal due to saturation effects, more than one slice can be sampled with the SENSE method within one TR without compromising SNR, spatial or spectral resolution. This also holds for conventional SI. However, some fast techniques such as multiecho SI require the full repetition time for the acquisition of several spin echoes. As a consequence, not only a short acquisition time per echo is required, leading to low spectral resolution, but also a longer repetition time, and thus a longer scan time, is needed when multiple slices are to be acquired. Thus, the total scan time increases with the number of slices. In multislice SENSE-SI all acquisition parameters can stay the same as in single slice SI, as long as the product of acquisition time and number of slices fits into the repetition time. For example, two spectroscopic imaging slices with a spectral resolution of 1.5 Hz and a bandwidth of 750 Hz can be easily acquired with a repetition time of 1.5 sec and no additional scan time with SENSE-SI. In this case, the reference scan needed for the coil sensitivities has to be done for each of the slices.

SENSE-SI is expected to be particularly useful at higher field strengths. The quality of SENSE metabolite images will clearly improve as the inherent SNR increases. This advantage may even facilitate spectroscopic imaging with enhanced spatial resolution. Furthermore, since multiple echoes are not required, the spatial resolution of SENSE-SI will not be degraded by the reductions in T_2 seen at higher field strengths. Due to its favorable performance at short T_2, SENSE-SI may also prove valuable for ^{31}P-SI. For this option, however, the determination of coil sensitivity maps poses a particular challenge yet to be investigated.

CONCLUSION

Sensitivity encoding with a receiver array has proven a powerful tool for fast spectroscopic imaging. The findings of this work demonstrate that, using SENSE, metabolite maps can be acquired substantially faster than with conventional SI methods alone, and without certain disadvantages inherent to other fast SI methods. This improvement is particularly promising as it adds to the potential value of metabolic imaging as a clinical tool. Without limiting the choice of the *k*-space sampling pattern or spatial or spectral resolution, it may be combined with existing fast SI methods for additional enhancement of scan speed or resolution. Furthermore, not depending on long T_2 relaxation times, SENSE-SI is a promising concept for high-field SI.

ACKNOWLEDGMENTS

The authors thank Johan Van den Brink and Rolf Lamerichs from Philips Medical Systems in Best, The Netherlands, for the impulse that lead to this work and for software support. We thank the Philips Research Laboratories in Hamburg for material support; in particular, the authors thank Christoph Leussler and Peter Röschmann, who built the six-element coil array, and Dr. Tobias Schäffter for providing the spectroscopic imaging phantom.

REFERENCES

1. Barker PB, Szopinski K, Horska A. Metabolic heterogeneity at the level of the anterior and posterior commissures. Magn Reson Med 2000;43: 348–354.
2. Vermathen P, Laxer KD, Matson GB, Weiner MW. Hippocampal structures: anterioposterior N-acetylaspartate differences in patients with epilepsy and control subjects as shown with proton MR spectroscopic imaging. Radiology 2000;214:403–410.
3. Carhuapoma JR, Wanh PY, Beauchamp NJ, Keyl PM, Hanley DF, Barker PB. Diffusion-weighted MRI and proton MR spectroscopic imaging in the study of secondary neuronal injury after intracerebral hemorrhage. Stroke 2000;31:726–732.
4. Fitzgerald KD, Moore GJ, Paulson LA, Steward CM, Rosenberg DR. Proton spectroscopic imaging of the thalamus in treatment-naïve pediatric obsessive-compulsive disorder. Biol Psychiatry 2000:47:174–182.
5. Scheidler J, Hricak H, Vigneron DB, Yu KK, Sokolov DL, Huang LR, Zadoulek CJ, Nelson SJ, Carroll PR, Kurhanewicz J. Prostate cancer: localization with three-dimensional proton MR spectroscopic imaging—clinicopathologic study. Radiology 1999;213:473–480.
6. Pfefferbaum A, Adalsteinsson E, Spielman D, Sullivan EV, Lim KO. In vivo spectroscopic quantification of the N-acetyl moiety, creatine, and choline from large volumes of brain gray and white matter: effects of normal aging. Magn Reson Med 1999;41:276–284.
7. Maudsley AA. Sensitivity in Fourier imaging. J Magn Reson 1986;68: 363–366
8. Brown TB, Kincaid BM, Ugurbil K. NMR chemical shift imaging in three dimensions. Proc Natl Acad Sci USA 1982;79:3523–3526.
9. Maudsley AA, Hilal SK. Spatially resolved high resolution spectroscopy by four-dimensional NMR. J Magn Reson 1983;51:147–152.

10. Duyn JH, Moonen CTW. Fast proton spectroscopic imaging of human brain using multiple spin-echoes. Magn Reson Med 1993;30:409–414.
11. Mansfield P. Spatial mapping of the chemical shift in NMR. Magn Reson Med 1984;1:370–386.
12. Posse S, Tedeschi G, Risinger R, Ogg R, LeBihan D. High speed 1H spectroscopic imaging in human brain by echo planar spatial-spectral encoding. Magn Reson Med 1995;33:34–40.
13. Sepponen RS, Sipponen JT, Tanttu JI. A method for chemical shift imaging: demonstration of bone marrow involvement with proton chemical shift imaging. J Comput Assist Tomogr 1984;8:585–587.
14. Guimaras AR, Baker JR, Jenkins BG, Lee PL, Weisskopf RM, Rosen BR, Gonzales RG. Echoplanar chemical shift imaging. Magn Reson Med 1999;41:877–882.
15. Norris DG, Dreher W. Fast proton spectroscopic imaging using the sliced k-space method. Magn Reson Med 1993;30:641–645.
16. Adalsteinsson E, Irarrazabal P, Topp S, Meyer C, Macovsci A, Spielman DM. Volumetric spectroscopic imaging with spiral-based k-space trajectories. Magn Reson Med 1998;39:889–898.
17. Pruessmann KP, Weiger M, Scheidegger MB, Boesiger P. SENSE: sensitivity encoding for fast MRI. Magn Reson Med 1999;42:952–962.
18. Dydak U, Weiger M, Pruessmann KP, Van den Brink J, Lamerichs R, Meier D, Boesiger P. Scan time reduction in spectroscopic imaging using SENSE. In: Proc 7th Annual Meeting ISMRM, Philadelphia, 1999. p 679.
19. Weiger M, Pruessmann KP, Boesiger P. 2D SENSE for faster 3D imaging. In: Proc 8th Annual Meeting ISMRM, Denver, 2000. p 152.
20. Schaeffter T, Boernert P, Leussler C, Carlsen IC, Leibfritz D. Fast 1H spectroscopic imaging using a multi-element head coil array. Magn Reson Med 1998;40:185–193.
21. Haase A, Frahm J, Haenicke W, Matthaei D. ^{1}H NMR chemical shift selective (CHESS) imaging. Phys Med Biol 1985;4:341–344.
22. Bottomley PA. Spatial localization in NMR spectroscopy in vivo. Ann NY Acad Sci 1987;508:333–348.
23. Dydak U, Weiger M, Pruessmann KP, Meier D, Boesiger P. Sensitivity encoded multi-echo spectroscopic imaging. In: Proc 8th Annual Meeting ISMRM, Denver, 2000. p 368.
24. Weiger M, Pruessmann KP, Leussler C, Röschmann P, Boesiger P. Specific coil design for SENSE: a six-element cardiac array. Magn Reson Med 2001;45:495–504.